JOURNAL OF PROPULSION AND POWER
Vol. 24, No. 5, September–October 2008

Detached-Eddy Simulation of a Louver-Cooling Scheme for Turbine Blades

C. X-Z. Zhang,* S. I. Kim,† and I. Hassan‡
Concordia University, Montréal, Québec H3G 1M8 Canada

DOI: 10.2514/1.35230

The performance of a louver-cooling scheme on a flat plate was analyzed using a detached-eddy-simulation turbulence model. It was assumed that the louver-cooling scheme was tested in a wind tunnel with the mainstream flow velocity of 20 m/s, equivalent to a Reynolds number of 16,200, based on the jet diameter. Turbulence closure was achieved by a realizable k-ε-based detached-eddy-simulation turbulence model. Solutions of two blowing ratios of 0.5 and 1 were successfully obtained by running parallel on 16 nodes on a computer cluster. The flowfields were found to be highly unsteady and oscillatory in nature, with the maximum fluctuation of the adiabatic effectiveness as high as 15% of the time-averaged value. It is shown that the fluctuations in the adiabatic effectiveness are mainly caused by the spanwise fluctuation of the coolant jet and the unsteady vortical structures created by the interaction of the jet and the mainstream.

Nomenclature

DR	=	density ratio, ρ_j/ρ_∞
d	=	diameter of the hole at the inlet, m
k	=	turbulent kinetic energy, m^2/s^2
m	=	blowing ratio, $\rho_j U_j/\rho_\infty U_\infty$
P	=	pressure, Pa
Q	=	nondimensional Q criterion, $q(d/U_\infty)^2$
q	=	Q criterion, $(\lvert\Omega_{ij}\rvert^2 - \lvert S_{ij}\rvert^2)/2$, $1/s^2$
S	=	strain rate, $S_{ij} = (u_{i,j} + u_{j,i})/2$, $1/s$
T	=	temperature, K
t	=	time, s
u	=	velocity component in the x direction, m/s
v	=	velocity component in the y direction, m/s
w	=	velocity component in the z direction, m/s
x	=	streamwise coordinate, m
y	=	vertical coordinate, m
z	=	spanwise coordinate, m
ε	=	dissipation rate of turbulent kinetic energy, m^2/s^3
η	=	local adiabatic film-cooling effectiveness, $(T_{aw} - T_\infty)/(T_j - T_\infty)$
θ	=	nondimensional temperature, $(T - T_j)/T_\infty - T_j)$
ρ	=	density, kg/m^3
τ	=	nondimensional time, tU_∞/d
Ω	=	vorticity, $\Omega_{ij} = (u_{i,j} - u_{j,i})/2$, $1/s$
ω	=	nondimensional vorticity, $\Omega d/U_\infty$

Subscripts

aw	=	adiabatic wall
j	=	jet
∞	=	mainstream conditions

Received 19 October 2007; revision received 2 May 2008; accepted for publication 3 May 2008.

*Graduate Student, Department of Mechanical and Industrial Engineering.
†Research Associate, Department of Mechanical and Industrial Engineering.
‡Associate Professor, Department of Mechanical and Industrial Engineering; IbrahimH@alcor.concordia.ca.

I. Introduction

THE efficiency and power output of gas turbines have been continually increasing due to more efficient turbine-blade-cooling techniques, such as film cooling, impingement cooling, and transpiring cooling. In addition to providing cooling to the gas turbine blades, film cooling is also widely used to cool combustion chambers. Generally, some small discrete holes are machined on a surface, through which cooler fluid was injected into the mainstream. After injection, the coolant will form a film to cover the downstream targeted surface, reducing heat load. Research into this jet-in-a-crossflow phenomenon has been extensive. Early studies were focused on circular holes on a flat plate. Shaped holes attracted much attention in the last two to three decades. The research into the fundamental problem of a circular hole on a flat plate is still being carried out, because the jet in a crossflow is still not fully understood. Most of the numerical studies are about steady simulation based on the Reynolds-averaged Navier–Stokes (RANS) approach. Because unsteady simulations are very computationally intensive, almost all of the studies related to the unsteady simulation were carried out within the last 10 to 15 years, thanks to ever-increasing computing power making the numerical calculation practical.

The majority of the numerical studies on film cooling have been based on the assumption that the flowfield is steady-state. However, experimental results by Fric and Roshko [1] revealed that the flowfield associated with a jet in a crossflow is highly unsteady and complex, with at least four different types of vortices. Therefore, the assumption of steady state, at best, is a rough approximation. It is widely accepted that the mixing processes downstream of the hole are highly anisotropic, because the turbulent diffusion is much stronger in the transverse direction than in the streamwise direction. This is possibly the cause of underprediction of jet spreading by the isotropic turbulence models. Roy et al. [2] performed numerical simulations using a finite-volume-based parallel solver called Cobalt with a Spalart–Allamaras (S–A)-based detached-eddy simulation (DES), which makes no such assumption of isotropy downstream of the hole. However, the prediction by DES in comparison with experimental data proved to be no more accurate than that of the RANS-model solution, which was attributed to the use of a symmetry boundary condition in the simulation, because the symmetry boundary might have inhibited the growth of three-dimensional asymmetric instability, deterring further mixing. In a paper by Kapadia and Roy [3], the symmetry boundary condition was abandoned and a periodic boundary condition was employed with a full computational domain of one period to capture the asymmetric vortical flow patterns. Improved cooling-effectiveness prediction was achieved and the DES solution was more realistic, because it captured the asymmetric features in temperature and velocity distribution.

Claiming the existing two-equation models failed to resolve the anisotropy and the dynamics of the highly complex flowfield created by the jet-in-a-crossflow interaction based on the literature, Tyagi and Acharya [4] studied film cooling using large-eddy simulation (LES), in which the dynamics of the larger scales in the flow are directly resolved. A uniform grid of $172 \times 102 \times 62$ was used to mesh the computational domain of the size of $17 \times 5 \times 6d$ with a periodic boundary condition used in the spanwise direction on the domain including one single hole. The velocity predictions at both blowing ratios of 0.5 and 1 are generally in good agreement with experimental data. The agreement of cooling effectiveness between predictions and experimental data was also good at a low blowing ratio of 0.5. Coherent structures were extracted using positive isosurfaces of the Laplacian of the pressure field. It was shown that the cooling effectiveness was intrinsically linked to the dynamics of the hairpin structures. All previously reported vortical structures were identified and all the discrepancies were attributed to the insufficient averaging of time-dependent fields and the uncertainties associated with boundary conditions.

Wegner et al. [5] used the LES methodology to investigate how turbulent mixing can be enhanced by varying the angle between the jet and the oncoming crossflow. In the LES model, all scales of motion and mixing smaller than a given filter width were removed by filtering the governing equations, whereas large scales were explicitly computed. A total grid size of 430,000 cells was used at the blowing ratio of 0.5 with a circular jet on a flat plate, because the jet does not penetrate far into the crossflow; hence, a large number of nodes in the wall-normal direction are not necessary to achieve a good resolution. It was demonstrated that the LES can well capture the flow and mixing features in jets in a crossflow, in comparison with experimental data.

Holloway et al. [6] studied the jet in a crossflow by considering new unsteady physics. A new in-house unsteady RANS-based turbulence model was developed and tested with other models against experimental data. They determined that current steady RANS turbulence models tend to underpredict jet-crossflow mixing. Therefore, it was believed that the inclusion of unsteady mechanisms should enhance predicted mixing rates and improve results. The meshes consisted of around 2 million finite volumes, and 15 iterations per time step proved to be adequate. In contrast to the steady simulations of film cooling (which indicated a significant overprediction of adiabatic effectiveness at high blowing ratios, especially in the near-hole region), the new approach did lead to an improvement in the effectiveness prediction in that the dramatic overprediction in the near-hole region was eliminated by the unsteady approach. There was still some quantitative disagreement with the experimental data for this case, however.

Guo et al. [7] performed LES simulations of a jet-in-a-crossflow problem to investigate the turbulent flow structures and vortex dynamics in film cooling on a flat plate. The jet in a crossflow of two inclination angles of 30 and 90 deg, along with two low blowing ratios of 0.1 and 0.48, was analyzed using a filtered Navier–Stokes equations solver. No separation along the leading edge of the jet hole was observed, because the blowing ratios tested were low. The results have to be viewed with caution, due to a lack of comparison with experimental data.

The literature survey shows that the jet in a crossflow is a very complicated mixing process between the jet and the mainstream. Counter-rotating vortex shedding is a dominating mechanism in determining the downstream cooling effectiveness. Therefore, the mixing process is highly unsteady and the steady-state assumption in the RANS approach may undermine the accuracy of its solutions. That may partly explain the discrepancies between the numerical predictions and the experimental data in a number of studies. In this study, numerical simulations using a DES turbulence model was performed for film holes on a flat plate, including a louver scheme. The louver scheme was first introduced by Immarigeon and Hassan [8] and subsequently refined by Zhang and Hassan [9,10] to show its full potential. All the work done to this scheme to date has been steady numerical simulations. This will be the first effort of unsteady simulation of this louver scheme using a DES turbulence model.

II. Turbulence Modeling and Boundary Conditions

The test conditions are based on the Sinha et al. [11] study, in which experiments were conducted in a closed-loop wind-tunnel facility. The test section is a flat plate made of polystyrene foam to reduce the conduction errors during the test. Cooler air was issued from a row of the holes, each 1.27 cm in diameter and spaced 3 diameters apart laterally. Thermocouples were positioned on the test surface to obtain the cooling-effectiveness data. The mainstream flow conditions were kept constant: a freestream velocity of 20 m/s at the inlet and a turbulence level of about 0.2%. Different blowing ratios were achieved by changing the plenum inlet mass flow rate. The louver-cooling scheme was tested under the same conditions numerically. The film-cooling-hole configurations are shown in Figs. 1a and 1b for the circular hole and the louver-cooling scheme, respectively.

The Reynolds number based on the hole diameter is 16,200; therefore, turbulent flow prevails. The flow is governed by conservation equations of continuity, momentum, and energy. In addition, a turbulence model is needed to reach a mathematical closure. In this study, the realizable k-ε-based DES model provided by FLUENT, Inc., was selected to carry out the simulations because a previous study [9] showed the superiority of this turbulence model over the other models in film-cooling applications. In the DES turbulence modeling, the unsteady realizable k-ε model is employed in the near-wall regions, whereas the same filtered realizable k-ε model is used in any other regions away from walls. The transport equations for k and ε in the realizable k-ε model are as follows:

$$\frac{\partial}{\partial t}(\rho k) + \frac{\partial}{\partial x_j}(\rho k u_j) = \frac{\partial}{\partial x_j}\left[\left(\mu + \frac{\mu_t}{\sigma_k}\right)\frac{\partial k}{\partial x_j}\right] + G_k + G_b - Y_k - Y_M + S_k \tag{1}$$

$$\frac{\partial}{\partial t}(\rho \varepsilon) + \frac{\partial}{\partial x_j}(\rho \varepsilon u_j) = \frac{\partial}{\partial x_j}\left[\left(\mu + \frac{\mu_t}{\sigma_\varepsilon}\right)\frac{\partial \varepsilon}{\partial x_j}\right] + \rho C_1 S_\varepsilon - \rho C_2 \frac{\varepsilon^2}{k + \sqrt{\nu\varepsilon}} + C_{1\varepsilon}\frac{\varepsilon}{k} C_{3\varepsilon} G_b + S_\varepsilon \tag{2}$$

Detailed information of the realizable k-ε model can be found in [12].

DES is a hybrid model that combines the efficiency of RANS and the accuracy of LES length scales to work under a single framework. DES works by applying a variable length scale that varies as a function of the distance to the nearest wall in the attached boundary layer and conforms with subgrid scale in the rest of the flow, including separated regions and the near wake [13]. In the realizable k-ε-based DES model, the RANS model is similar to the realizable k-ε model, with the exception of the dissipation term in the k equation. In the DES model, the realizable k-ε dissipation term is modified such that

$$Y_k = \frac{\rho k^{3/2}}{l_{\text{DES}}} \tag{3}$$

where

$$l_{\text{DES}} = \min(l_{\text{RKE}}, l_{\text{LES}}), \qquad l_{\text{RKE}} = \frac{k^{3/2}}{\varepsilon}, \qquad l_{\text{LES}} = C_{\text{DES}}\Delta$$

where C_{DES} is a calibration constant used in the DES model and has a value of 0.61, and Δ is the maximum local grid spacing $(\Delta x, \Delta y, \Delta z)$ [14].

Figure 1c shows the computational domain and boundary conditions. The computational model assumes infinite rows of film-cooling holes on a flat plate, so that the endwall effects can be neglected. At the upstream inlet, a constant velocity of 20 m/s normal to the inlet boundary was applied, with the freestream turbulence being 0.2% as in the experimental work. At the outlet, a pressure boundary condition was imposed. The domain extends $20d$ from the bottom test surface, far enough such that a free-slip boundary condition or zero shear stress may be applied. If the computational domain is only half of a period, symmetry boundary conditions are imposed at both

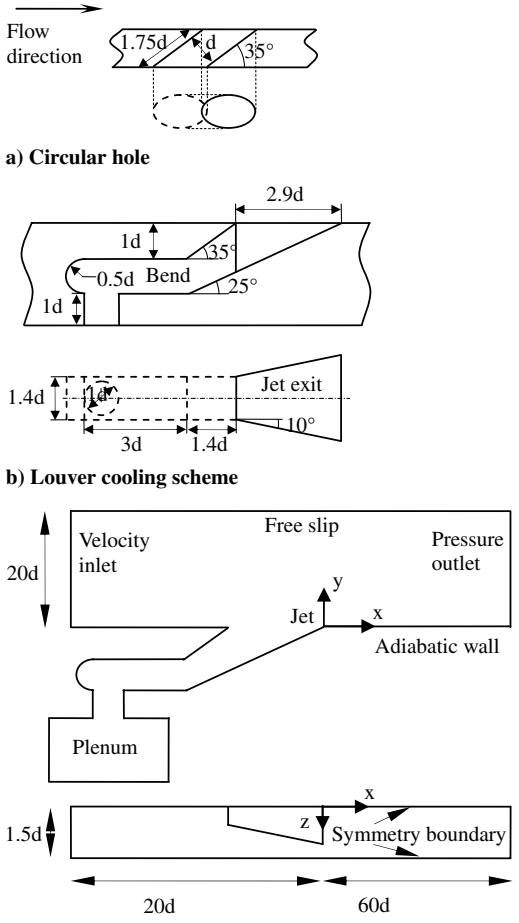

Fig. 1 Film-cooling configurations and computational domain with boundary conditions.

the central plane and at the $1.5d$ plane in the streamwise direction. If a full domain is employed, a periodic boundary condition will be applied. At the bottom wall, as well as the other walls, an adiabatic-wall boundary condition with no slip was imposed. The temperatures at the mainstream and plenum inlets were specified at 300 and 150 K, respectively, which gives a coolant-to-mainstream density ratio of 2. All these boundary conditions were based on Sinha et al. [11].

Multiblock mostly structured meshes were created to fully resolve the features of the flowfield, with most of the cells concentrated in areas of large variable gradients, because a hexahedron is more efficient to fill a volume than a tetrahedron. When used appropriately, this method successfully captured the jet-liftoff effect in a traditional circular jet in a crossflow over a flat plate. Details of this methodology can be found in [9,10]. It should be noted that this is the only steady numerical study clearly demonstrating the successful capturing of the jet-liftoff effect in the circular hole on a flat plate. This numerical procedure will be extended to study film-cooling holes in an unsteady DES simulation.

The grids contain between 0.3 and 0.8 million cells, depending on whether it is a half- or full-meshed domain. This number of cells has proven to be sufficient to reach a grid-independent solution as outlined in [9]. The cases were first run on a workstation for the steady solution with a CPU of 3 GHz and RAM of 3 GB. It took around 2000 iterations to reach convergence, approximate 20 h of computing time. The case and data files were subsequently transferred to a supercomputer, a high-performance computing (HPC) cluster, for further computation. After being switched to an unsteady simulation with the steady results as the initial solution, the simulation continued to run parallel on 16 nodes with 16-GB memory on the cluster. The iterations were stopped to check whether steady state was statistically reached. If the answer was positive, data sampling for time statistics was launched for more iterations to calculate the time-averaged results. It took two weeks of intensive parallel computing on 16 nodes on the cluster to get one solution.

III. Results and Discussion

A. Time-Step Size and Number of Subiterations

The time-step size in unsteady flow analysis affects the maximum frequency that can be resolved in the flow. Four different time steps from $\Delta t = 1 \times 10^{-4}$ to 1×10^{-6} s were tested, as shown in Fig. 2a, in which the velocity–time history at points 2, 0.4, and $0.08d$ for the cylindrical jet was plotted. The amplitude, frequency, and mean value of the velocity fluctuations for different time-step sizes were compared. As a result, $\Delta t = 1 \times 10^{-5}$ s is capable of capturing the unsteady features of the flow and should be sufficient (Kim et al. [15]). The number of subiterations at each time step also has a big impact on the final results. Therefore, it is very important to ensure that convergence is reached at one time step before marching to the next time step. Otherwise, the errors caused by an insufficient number of iterations at each time step (not fully converged solution at each time step) will add up and eventually contaminate the final solution. In this study, different numbers of subiterations were tested and Fig. 2b shows the result. In addition, at each time step, the solution residuals dropped at least 3 orders of magnitude. After comparing the results by different numbers of subiterations, it was concluded that the number of 30 iterations per time step was adequate.

B. Effect of Computational Domains

When a half-domain was used, symmetry boundary conditions were imposed on the center plane and the $z/d = 1.5$ plane. The use of

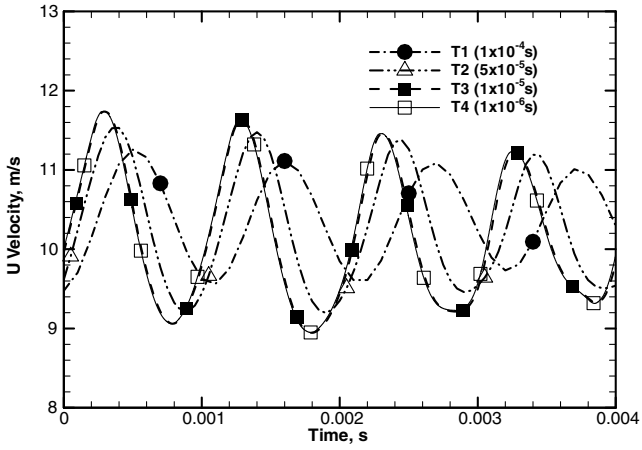

a) Test of the size of time steps

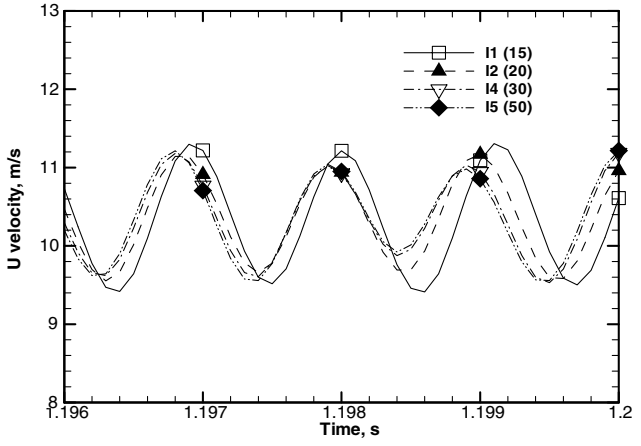

b) Test of the number of subiterations

Fig. 2 Test of the size of time steps and number of subiterations.

the symmetry boundary condition can be considered as a limitation of the unsteady simulation, because it prevents the possibility of capturing the unsteady asymmetric vortical flow patterns in the spanwise direction. To evaluate the effects of domain size, unsteady simulations using a half-domain with symmetry boundary conditions and a full domain with a periodic boundary condition were performed.

Instantaneous temperature contours and the corresponding velocity vector distributions at $x/d = 5$ plane are shown in Fig. 3. Both sides of the symmetric line are plotted to depict the dominant bound vortical structures for the case with a half-domain (Fig. 3a). In contrast to the case with a half-domain, Fig. 3b shows asymmetric distribution in nature from the full-domain computation. The coolant of the case with a full domain exhibits unsteady spanwise fluctuations, whereas the computation with a half-domain could not capture the full fluctuating in the spanwise direction. The unsteady simulation with a full domain is thus required to accurately predict lateral spreading of the coolant for a film-cooling flow as well as unsteady three-dimensional flow structures. Hence, a full computational domain with periodic boundary conditions was used throughout the remaining computations.

C. Comparison with Experimental Measurement

Figure 4a shows the comparison between experimental and computational data of film-cooling effectiveness along the centerline for the cylindrical jet at the blowing ratio of 1. At high blowing ratios, the coolant jets lift off from the surface. The steady predictions of other researchers, Leylek and Zerkle [16], Mulugeta and Patankar [17], Ferguson et al. [18], and Walters and Leylek [19], failed to capture the jet-liftoff phenomenon near downstream of the injection hole (Fig. 4a), possibly due to either inadequate grid density or turbulence modeling. Ferguson et al. [18] and Walters and Leylek [19] employed unstructured meshes, which makes it very difficult to have adequate grid concentration at the jet exit area. Even when the grid concentration was adequate, the standard k-ε model completely missed the jet liftoff, as shown in [9], and the standard k-ε model was used in [16,17,19]. However, the present DES prediction shows a greater rate of decrease in effectiveness immediately downstream of the injection hole, due to the jet liftoff and hot-entrainment flows. The time-averaged distribution of the laterally averaged film-cooling effectiveness is shown in Fig. 4b. Also shown are the experimental data of Sinha et al. [11] and other numerical results at the same blowing ratio and with the same geometry. The present realizable k-ε-based DES simulation gives an improved prediction, compared with the S–A-based DES result of Roy et al. [2] (Fig. 4b). The ability of DES simulation to capture the jet liftoff and unsteady behaviors is desirable.

D. Time-Averaged Film-Cooling Characteristics

Unsteady simulations for the louver-cooling scheme were performed in this study using the realizable k-ε-based DES model for the blowing ratios of 0.5 and 1.0. A comparison between the steady and unsteady time-averaged results and the experimental data of the traditional cylindrical hole and forward and lateral shaped holes was made. The steady results were obtained from the steady RANS (realizable k-ε model) simulations. The present time-averaged results were obtained from the averaging of unsteady data during 15,000 time steps.

Figure 5 shows the centerline effectiveness at the blowing ratios of 0.5 and 1.0 for the louver scheme. The difference of cooling effectiveness between the steady and unsteady time-averaged results

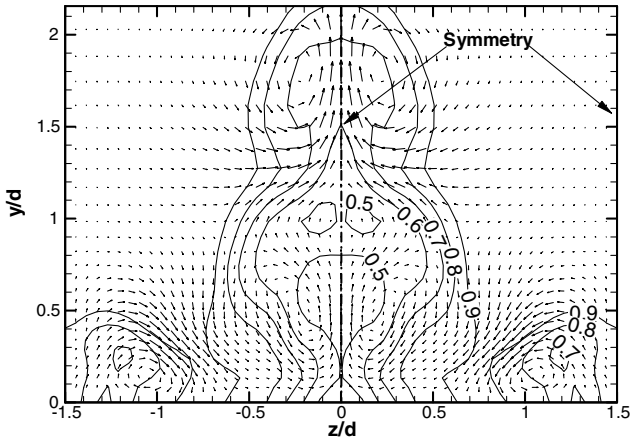

a) Half-domain with symmetric boundary condition

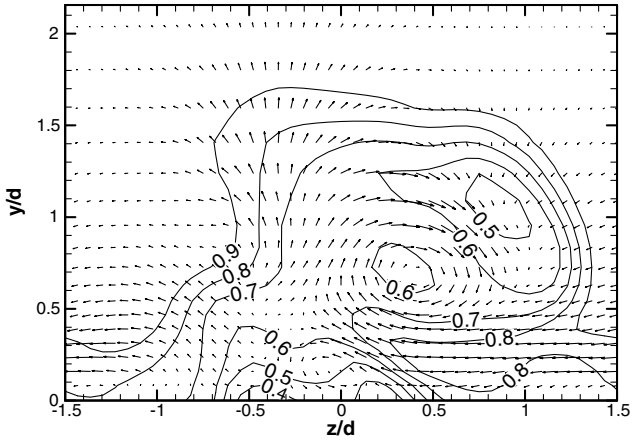

b) Full domain with periodic boundary condition

Fig. 3 Instantaneous temperature contours and velocity vectors at $x/d = 5$ plane for the louver scheme.

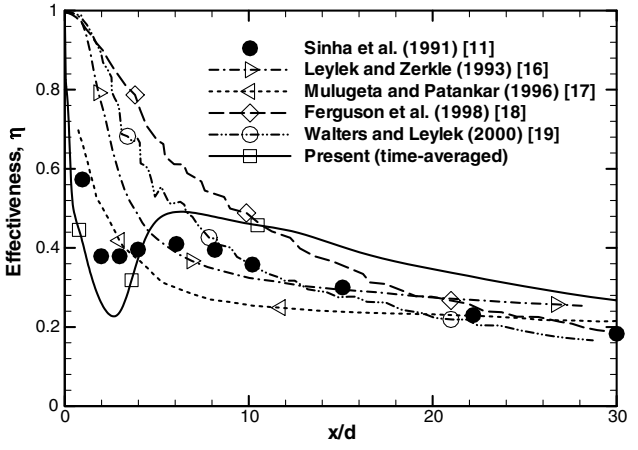

a) Along the centerline

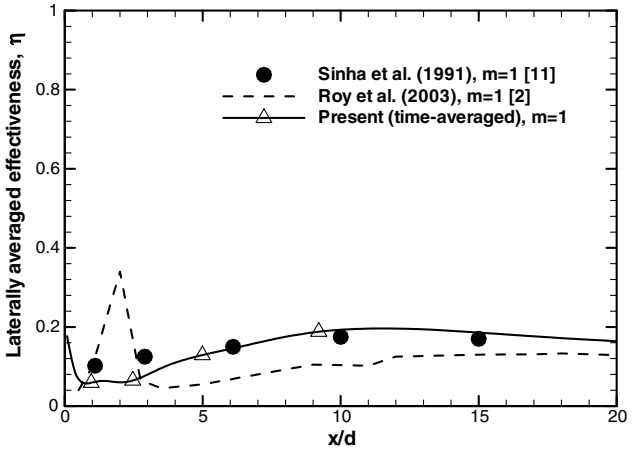

b) Laterally averaged η

Fig. 4 Comparison between experimental and computational values of η for the cylindrical jet.

can be seen. Also shown are the experimental data of the traditional cylindrical holes by Sinha et al. [11] and forward and lateral shaped holes by Yu et al. [20]. For the blowing ratio of 0.5 (Fig. 5a), the centerline effectiveness is at the same level for both the traditional cylindrical hole and the louver-cooling scheme, based on the numerically predicted results, because both jets stay attached to the surface after injection. The unsteady fluctuation of the coolant jet for the blowing ratio of 0.5 is relatively weak. Consequently, the time-averaged centerline effectiveness is almost the same as the steady result. For the blowing ratio of 1.0 (Fig. 5b), the jets in the Sinha et al. [11] case lift off from the surface, causing a sharp drop in effectiveness immediately downstream of the injection. However, in the louver scheme, the jets remain attached to the surface and the effectiveness gradually decreases in the streamwise direction. The time-averaged centerline effectiveness is lower than that of steady prediction, in contrast to the case of the 0.5 blowing ratio. A higher unsteady fluctuation of the coolant jet in the spanwise direction occurs, causing a wider spreading of coolant and a lower level of centerline effectiveness than that of the steady result.

The effect of the unsteadiness in the spanwise direction on film-cooling effectiveness can be seen easily in Fig. 6, which shows the effectiveness distribution in the spanwise direction. At the blowing ratio of 0.5, the effectiveness for both steady and unsteady (time-averaged) predictions is almost the same in the central region. Only a little more spread of coolant is observed in the time-averaged results. In the case of a 1.0 blowing ratio, the time-averaged local effectiveness of the louver scheme is lower than that of steady prediction in the central region, whereas it is higher in the outer region. The time-averaged effectiveness of the louver scheme is still higher than that of the cylindrical jets. Moreover, the time-averaged effectiveness for the louver scheme along the $x/d = 15$ line is almost uniform, which is considered more realistic.

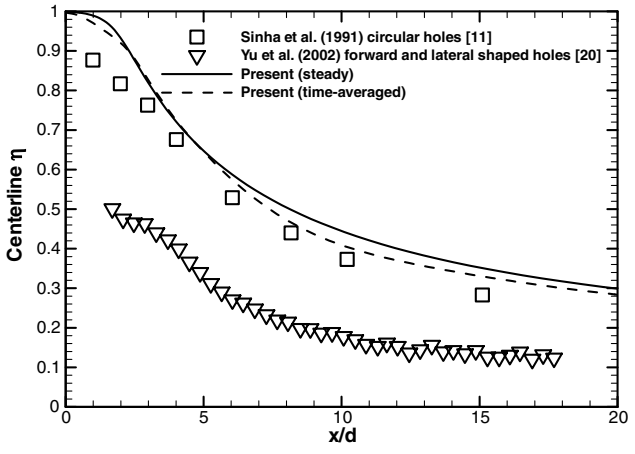

a) DR = 2, m = 0.5

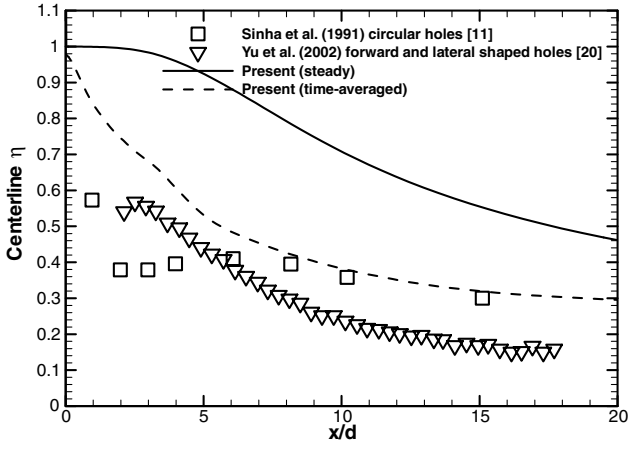

b) DR = 2, m = 1

Fig. 5 Centerline η for the louver scheme.

Figure 7 shows the comparison of laterally averaged effectiveness between different cooling schemes: namely, traditional circular holes by Sinha et al. [11], forward diffused holes by Bell et al. [21], both forward and lateral shaped holes by Yu et al. [20], straight fan-shaped holes by Dittmar et al. [22], fan-shaped holes by Saumweber et al. [23], and forward–lateral diffused holes by Taslim and Khanicheh [24]. The DES time-averaged result shows a lower effectiveness distribution at high blowing ratios and a higher effectiveness at low blowing ratios than that of the steady result, possibly the result of a wider spreading of the coolant in the spanwise direction in the DES unsteady solution (see Fig. 6). The decay of adiabatic film-cooling effectiveness of the steady simulation seems to be overpredicted on the test surface. The unsteady DES simulation may provide more reasonable prediction, especially for high blowing ratios. The time-averaged result of laterally averaged effectiveness for the louver scheme is still the highest, when some cooling schemes such as the circular holes undergo liftoff at the high blowing ratio of 1.

E. Unsteady Flow Characteristics

The nondimensional temperature distributions, including the instantaneous, time-averaged, and steady results, at the center plane in the wake region for both the cylindrical jet and the louver-cooling scheme are presented in Figs. 8 and 9, respectively. The instantaneous picture shows a highly unsteady mixing layer (Figs. 8a and 9a). The hot spot immediately downstream of the jet exit, caused by a coolant jet liftoff and hot-entrainment flows, can be seen for the cylindrical jet (Fig. 8a). A comparison between Figs. 8a and 9a reveals that under the same blowing ratio, the coolant-mainstream mixing process in the shear layer is more intense for the cylindrical than for the louver scheme. Most of the mixing takes place before x/d of 10, after which the coolant is pretty much settled, especially

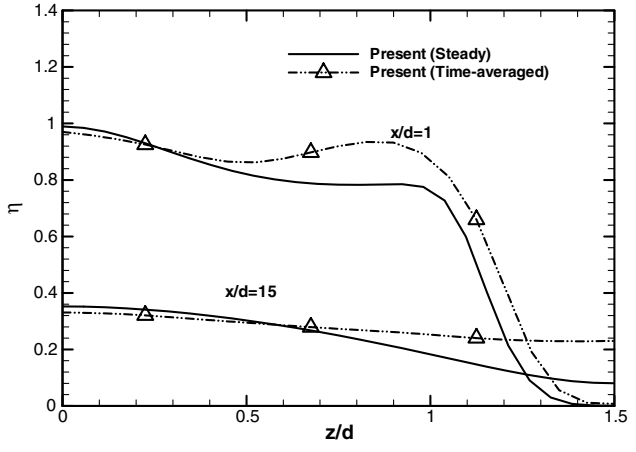

a) DR = 2, m = 0.5

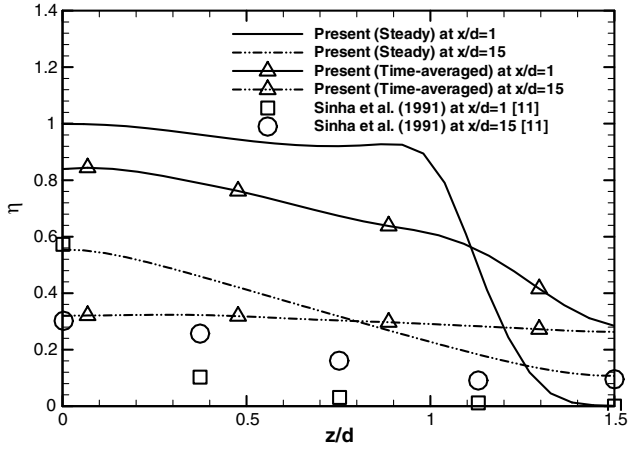

b) DR = 2, m = 1

Fig. 6 Comparison of local η for the louver scheme with the cylindrical jet.

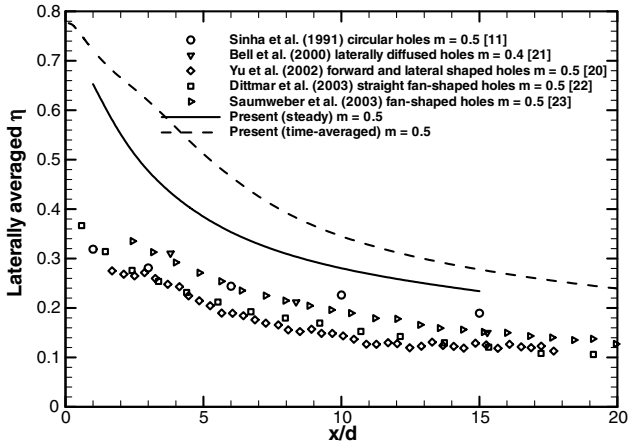

a) Low blowing ratios

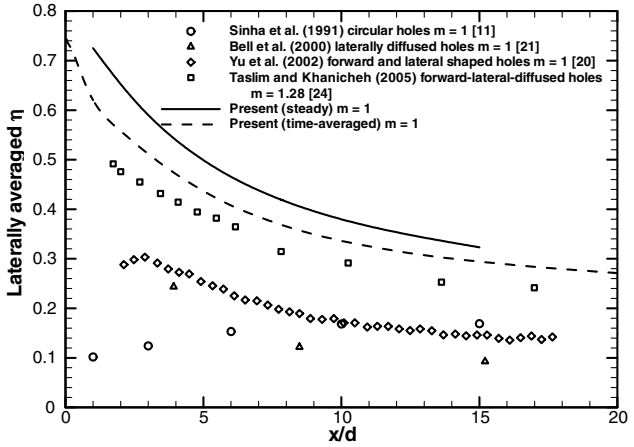

b) High blowing ratios

Fig. 7 Comparison of laterally averaged η between the louver scheme and other schemes.

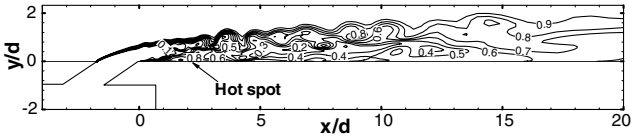

a) Instantaneous

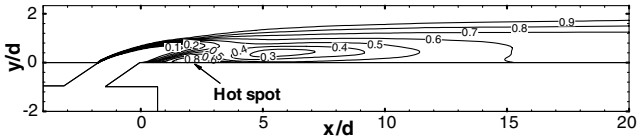

b) Time-averaged

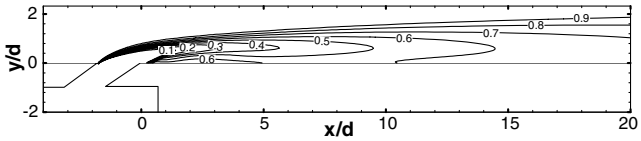

c) Steady

Fig. 8 Nondimensional temperature θ distributions at the center plane ($m = 1$) for the cylindrical jet.

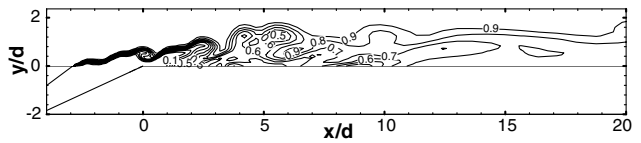

a) Instantaneous

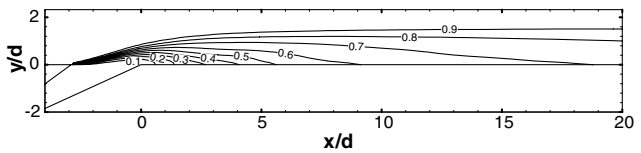

b) Time-averaged

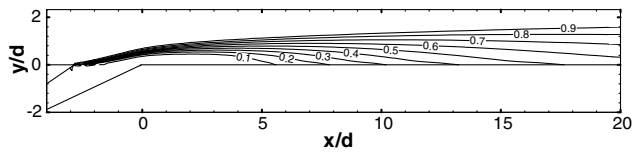

c) Steady

Fig. 9 Nondimensional temperature θ distributions at the center plane ($m = 1$) for the louver scheme.

for the louver scheme. The unsteadiness enhances the mixing process in the wake region and enlarges the mixing layer for the louver scheme. Contrary to the steady temperature distribution with a relatively thinner coolant layer near downstream of the injection and a longer low-temperature region (Fig. 9c), the time-averaged result reveals an intensified mixing layer with relatively thicker and more diffused coolant (Fig. 9b).

Figure 10 shows the instantaneous, time-averaged, and steady distribution of the adiabatic film-cooling effectiveness on the test surface at the blowing ratio of 1 for the louver scheme. The instantaneous result shows the highly disturbed distribution in the spanwise direction. The film is locally broken up, even at the core of the downstream region not far from the jet exit. That allows the hot fluid to tuck in close to the wall, locally diminishing the adiabatic film-cooling effectiveness. In the time-averaged result (Fig. 10b), it can be seen that the film-cooling effectiveness of the unsteady result is laterally more uniform than that of the steady result (Fig. 10c), and the cooling effectiveness is symmetric in the spanwise direction, as expected.

The Q criterion $q = (|\Omega_{ij}|^2 - |S_{ij}|^2)/2$ was used to identify coherent vortical structures. It indicates the balance between the rotation rate and the strain rate. Positive Q isosurfaces identify areas in which the strength of rotation surpasses the strain, thus making those surfaces eligible as vortex envelopes (Dubief and Delcayre [25]). A snapshot of typical coherent vortical structures of the cylindrical jet is shown in Fig. 11, in which a weak horseshoe vortex, counter-rotating vortex pair, inner vortices (vortex tubes), and downstream hairpin coherent structures can be identified by the Q criterion. Inner vortices, parts of vortex tubes, issued from the coolant injection hole play an important role in the jet mixing process and the jet-liftoff phenomena in the near-downstream region.

To clearly observe the coherent structures of the film-cooling flow for the louver scheme, the instantaneous normalized vorticity field at the center plane at $m = 1$ is plotted in Fig. 12. The roller vortices can be clearly identified in this figure. A time sequence of the coherent structures is shown in Fig. 13. The coherent structures are represented as a positive isosurface of the Q criterion ($Q = 1$). In the louver scheme, the coolant issued from the plenum impinges on the wall perpendicularly, is then redirected from the vertical to horizontal direction, and finally goes through an increasing cross-sectional area and an inclined path. The primary roll-up vortices due to the impingement of a vertical jet can be seen in the contours of spanwise vorticity component ω_z (Fig. 12). The vertical jet is a little tilted due to the bend. The inclined vortical flow is disturbed in passing through the flared and inclined path. The shear layer and roller vortices (negative vorticity patches) come from the leading edge of the jet exit. These roller vortices begin early to be shed over the coolant jet exit. Thus, the hairpin coherent structure occurs from the middle of the jet exit region (Fig. 13). The hairpin coherent structure is identified as the primary large-scale structure, as in the case of the cylindrical jet. The large-scale roll-up vortical structures are dissipated through the bent and flared path. In contrast to the case of the cylindrical jet, the inner

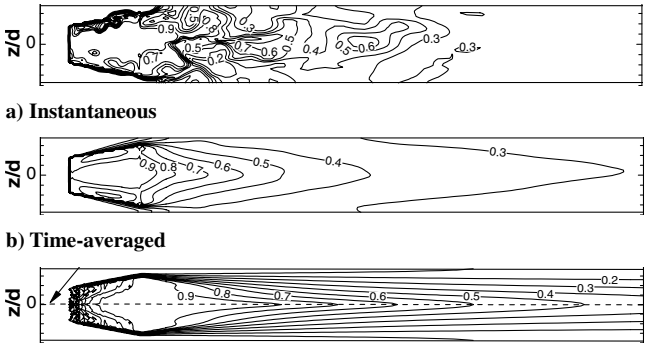

Fig. 10 Effectiveness distribution on the test surface for the louver scheme ($m = 1$).

vortex tubes and horseshoe vortex do not appear in the case of the louver scheme. The hairpin vortex structures for the louver scheme (Fig. 13a) are significantly smaller than those of the cylindrical jet (Fig. 11). They also break up and are dissipated earlier, shortly after injection for the louver scheme. Therefore, the jet liftoff is avoided and no significant hot spots are observed for the louver scheme at the blowing ratio of 1.

To identify the turbulent frequency spectrum of the vortical structures and mixing phenomenon, fast Fourier transform (FFT) analyses were conducted using the time-variant velocity components (u, v, w) at different locations. Figures 14 and 15 show the FFT

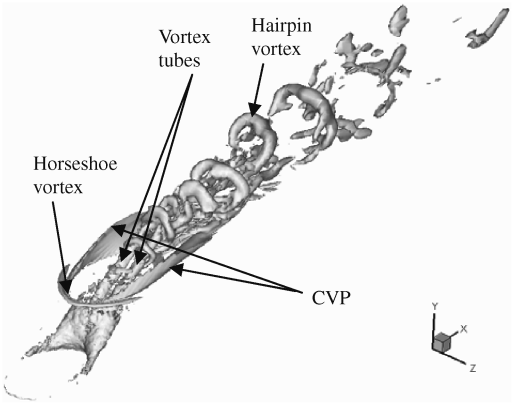

Fig. 11 Typical coherent structures in the inclined cylindrical jet in a crossflow (CVP denotes a counter-rotating vortex pair).

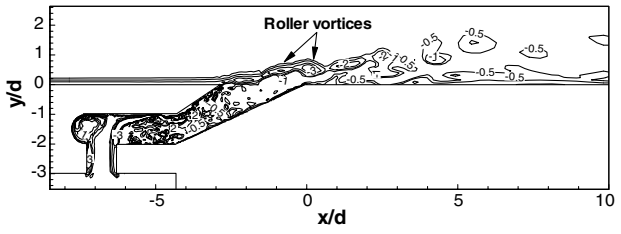

Fig. 12 Instantaneous normalized vorticity ω_z at the center plane for the louver scheme.

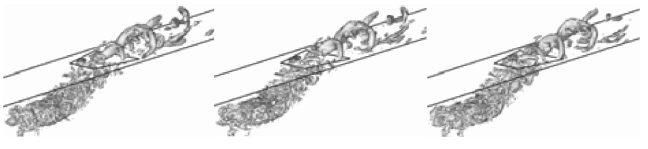

a) At an instant, τ_0 **b) At $\tau_0 + 0.8$** **c) At $\tau_0 + 1.6$**

Fig. 13 Snapshots of the coherent structures for the louver scheme at $m = 1$.

frequency spectrum for the velocity components at several points. For the cylindrical jet, one distinct dominant frequency is observed at the coolant exit plane (Fig. 14a). However, several distinct peaks can be observed for the louver scheme (Fig. 14c), due to more complex geometry than the cylindrical hole. The vortical structures are dissipated and the turbulent fluctuation increases through the louver scheme (Fig. 13). It causes a broad band of peaks at low, as well as at high, frequencies for the cases of both $m = 0.5$ and 1.0. However, as mentioned before, the case of a high blowing ratio of 1 shows higher unsteadiness and consequently has a higher amplitude than that of the low blowing ratio of 0.5. The low dominant frequencies (Fig. 15c) for the high blowing ratio of 1 are believed to be related to the unsteady motions of the large-scale coherent vortical structures. The different magnitudes of the velocity components, shown in Figs. 14 and 15, support the statement of anisotropic turbulence in the wake region.

IV. Conclusions

The performance of a louver-cooling scheme was studied by carrying out unsteady numerical simulations using a realizable k-ε-based DES turbulence model. As a validation, an unsteady analysis was first performed for a traditional cylindrical hole on a flat plate. A comparison with the experimental data shows that the jet liftoff was captured in the numerical prediction. The prediction of the lateral spreading of the jet after injection was also more realistic in the DES unsteady analysis than that of the steady analysis. One of the more important findings from this unsteady analysis is that the strong fluctuations and unsteadiness of the interaction between the jet and the mainstream can be captured very well, particularly the coolant fluctuation and the vortical structures in the spanwise direction, which will be impossible to capture in steady analysis.

1) The unsteady analysis captured the jet liftoff at high blowing ratios for the cylindrical holes on a flat plate. However, the jet-liftoff effect was exaggerated in the unsteady prediction. Overall, the

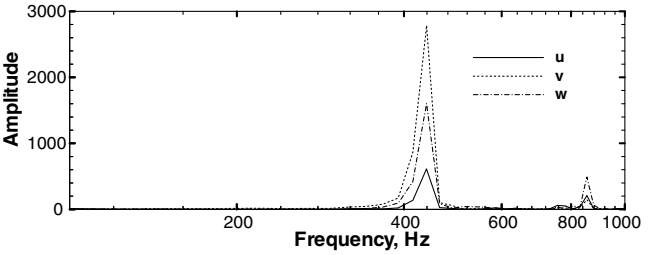

a) Circular hole, m = 1.0

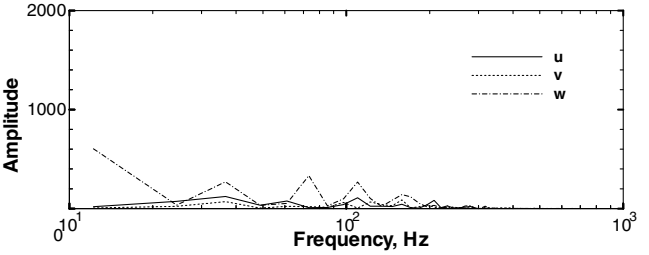

b) Louver scheme, m = 0.5

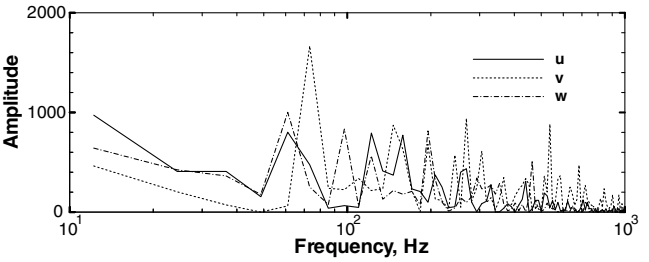

c) Louver scheme, m = 1.0

Fig. 14 FFT spectrum of time-variant velocity components on coolant exit plane.

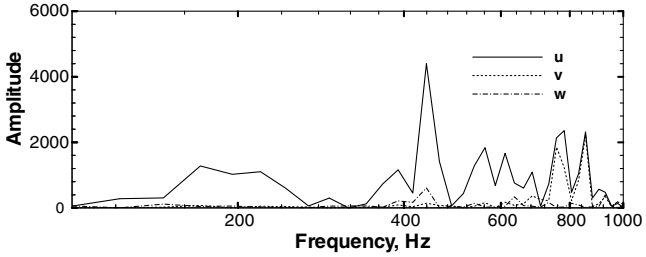

a) At (3d, 1d, 0), circular hole, m = 1.0

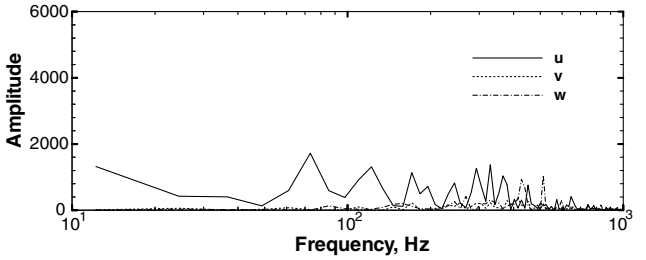

b) At (3d, 0.5d, 0.5d), louver scheme, m = 0.5

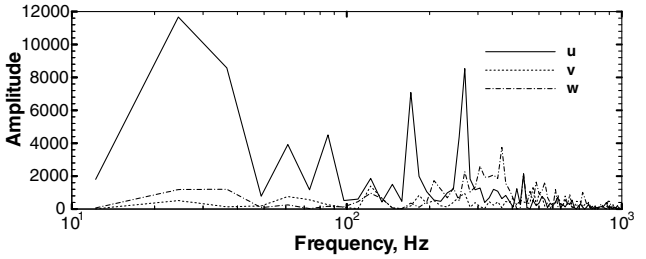

c) At (3d, 0.5d, 0.5d), louver scheme, m = 1.0

Fig. 15 FFT spectrum of time-variant velocity components downstream.

prediction of cooling effectiveness by the unsteady analysis is not significantly more accurate than that of steady analysis.

2) The unsteady analysis predicted more realistic lateral spreading of the jet than did the steady analysis, the biggest advantage of the unsteady analysis over its steady counterpart. To capture the unsteadiness and vortical structures of the jet in a crossflow, unsteady analysis is required.

3) Considering the cost in terms of computing resources and the accuracy of the unsteady analysis, unsteady analysis is not recommended for most practical industrial applications. The current computing power is still the largest limiting factor preventing unsteady analysis from finding wide applications.

References

[1] Fric, T. F., and Roshko, A., "Vortical Structure in the Wake of a Transverse Jet" *Journal of Fluid Mechanics*, Vol. 279, Nov. 1994, pp. 1–47. doi:10.1017/S0022112094003800

[2] Roy, S., Kapadia, S., and Heidmann, J. D., "Film Cooling Analysis Using DES Turbulence Model," American Society of Mechanical Engineers Paper GT-2003-38140, 2003.

[3] Kapadia, S., and Roy, S., "Detached Eddy Simulation of Turbine Blade Cooling," AIAA Paper AIAA-2003-3632, 2003.

[4] Tyagi, M., and Acharya, S., "Large Eddy Simulation of Film Cooling Flow From an Inclined Cylindrical Jet," *Journal of Turbomachinery*, Vol. 125, No. 4, 2003, pp. 734–742. doi:10.1115/1.1625397

[5] Wegner, B., Huai, Y., and Sadiki, A., "Comparative Study of Turbulent Mixing in Jet in Cross-Flow Configurations Using LES," *International Journal of Heat and Fluid Flow*, Vol. 25, No. 5, 2004, pp. 767–775. doi:10.1016/j.ijheatfluidflow.2004.05.015

[6] Holloway, D., Walters, D. K., and Leylek, J. H., "Computational Study of Jet-in-Crossflow and Film Cooling Using a New Unsteady-Based Turbulence Model," American Society of Mechanical Engineers Paper GT-2005-68155, 2005.

[7] Guo, X., Schroder, W., and Meinke, M., "Large-Eddy Simulations of Film Cooling Flows," *Computers and Fluids*, Vol. 35, No. 6, 2006, pp. 587–606. doi:10.1016/j.compfluid.2005.02.007

[8] Immarigeon, A., and Hassan, I., "An Advanced Impingement/Film Cooling Scheme for Gas Turbines—Numerical Study," *International Journal of Numerical Methods for Heat and Fluid Flow*, Vol. 16, No. 4, 2006, pp. 470–493. doi:10.1108/09615530610653091

[9] Zhang, X. Z., and Hassan. I., "Film Cooling Effectiveness of an Advanced-Louver Cooling Scheme for Gas Turbines," *Journal of Thermophysics and Heat Transfer*, Vol. 20, No. 4, 2006, pp. 754–763. doi:10.2514/1.18898

[10] Zhang, X. Z., and Hassan, I., "Numerical investigation of heat transfer on film cooling with shaped holes," *International Journal of Numerical Methods for Heat and Fluid Flow*, Vol. 16, No. 8, 2006, pp. 848–869. doi:10.1108/09615530610702032

[11] Sinha, A. K., Bogard, D. G., and Crawford, M. E., "Film-Cooling Effectiveness Downstream of a Single Row of Holes with Variable Density Ratio," *Journal of Turbomachinery*, Vol. 113, No. 3, 1991, pp. 442–449. doi:10.1115/1.2927894

[12] Shih, T.-H., Liou, W. W., Shabbir, A., Yang, Z., and Zhu, J., "A New k-ε Eddy-Viscosity Model for High Reynolds Number Turbulent Flows —Model Development and Validation," *Computers and Fluids*, Vol. 24, No. 3, 1995, pp. 227–238. doi:10.1016/0045-7930(94)00032-T

[13] Shur, M., Spalart, P. R., Strelets, M., and Travin, A., "Detached-Eddy Simulation of an Airfoil at High Angle of Attack," *Engineering Turbulence Modelling and Experiments 4*, Elsevier, New York, May 1999, pp. 669–678.

[14] *FLUENT 6.3 User's Guide*, Fluent, Inc., Lebanon, NH, Sept. 2006.

[15] Kim, S., Zhang, X. Z., and Hassan, I., "Unsteady Simulation of Film Cooling Flow from an Inclined Cylindrical Jet," American Society of Mechanical Engineers Paper HT2007-32401, 2007.

[16] Leylek, J. H., and Zerkle, R. D., "Discrete-Jet Film Cooling: A Comparison of Computational Results with Experiments," American Society of Mechanical Engineers Paper 93-GT-207, 1993.

[17] Mulugeta, K. B., and Patankar, S. V., "A Numerical Study of Discrete-Hole Film Cooling," American Society of Mechanical Engineers Paper 96-WA/HT-8, 1996.

[18] Ferguson, J. D., Walters, D. K., and Leylek, J. H., "Performance of Turbulence Models and Near-Wall Treatments in Discrete Jet Film Cooling Simulations," American Society of Mechanical Engineers Paper 98-GT-438, 1998.

[19] Walters, D. K., and Leylek, J. H., "A Detailed Analysis of Film Cooling Physics, Part 1: Streamwise Injection with Cylindrical Holes," *Journal of Turbomachinery*, Vol. 122, No. 1, 2000, pp. 102–112. doi:10.1115/1.555433

[20] Yu., Y., Yen, C. H., Shih, T. I. P., and Chyu, M. K., "Film Cooling Effectiveness and Heat Transfer Coefficient Distributions Around Diffusion Shaped Holes," *Journal of Heat Transfer*, Vol. 124, No. 5, 2002, pp. 820–827. doi:10.1115/1.1418367

[21] Bell, C. M., Hamakawa, H., and Ligrani, P. M., "Film Cooling from Shaped Holes," *Journal of Heat Transfer*, Vol. 122, No. 2, 2000, pp. 224–232. doi:10.1115/1.521484

[22] Dittmar, J., Schulz, A., and Wittig, S., "Assessment of Various Film-Cooling Configurations Including Shaped and Compound Angle Holes Based on Large-Scale Experiments," *Journal of Turbomachinery*, Vol. 125, No. 1, 2003, pp. 57–64. doi:10.1115/1.1515337

[23] Saumweber, C., Schulz, A., and Wittig, S., "Free-Stream Turbulence Effects on Film Cooling with Shaped Holes," *Journal of Turbomachinery*, Vol. 125, No. 1, 2003, pp. 65–73. doi:10.1115/1.1515336

[24] Taslim, M. E., and Khanicheh, A., "Film Effectiveness Downstream of a Row of Compound Angle Film Holes," *Journal of Heat Transfer*, Vol. 127, No. 4, 2005, pp. 434–440. doi:10.1115/1.1865222

[25] Dubief, Y., and Delcayre, F., "On Coherent-Vortex Identification in Turbulence," *Journal of Turbulence*, Vol. 1, No. 11, 2000, pp. 1–22. doi:10.1088/1468-5248/1/1/011

F. Liu
Associate Editor